Available online at www.sciencedirect.com
ScienceDirect
Polymer 47 (2006) 7397–7405
polymer
www.elsevier.com/locate/polymer

Fluorescence and molecular dynamics to study the intramolecular energy transfer in *N*-vinyl carbazole/styrene copolymers of different molar compositions

Nicolás Gatica, Gema Marcelo, Francisco Mendicuti*

Departamento de Química Física, Universidad de Alcalá, ctra. Madrid-Barcelona Km 33.6, 28871 Alcalá de Henares, Madrid, Spain

Received 5 June 2006; received in revised form 15 August 2006; accepted 16 August 2006
Available online 7 September 2006

Abstract

Emission spectra, fluorescence polarization, quenching and lifetime measurements were performed on dilute solutions of poly(*N*-vinyl carbazole) and *N*-vinyl carbazole/styrene copolymers to study the intramolecular energy transfer between carbazole groups along the polymer chain. Fluorescence anisotropy values for the samples dissolved in a PMMA solid matrix and quenching measurements in toluene by CCl_4 were used to estimate the efficiency of energy transfer as a function of the monomer molar composition. Analysis of the experiments suggests that the copolymer with the highest carbazole content, which corresponds to the highest amount of carbazole excimers, does not show the highest energy transfer efficiency. Intramolecular excimers which strongly increase with the carbazole content and that are mainly due to carbazole–carbazole monomer sequence interactions undoubtedly act as energy transfer traps. Molecular dynamics simulations on isotactic and syndiotactic copolymer fragments were used for obtaining different parameters related to the energy transfer process as a function of the number of styrene monomer units between vinyl carbazole ones.

Keywords: Excimers; Energy transfer; Poly(*N*-vinyl carbazole)

1. Introduction

There are many possible applications for photoconductive polymers [1]. A prototype of these materials is the poly(*N*-vinyl carbazole), PVCz, which is also one of the polymers whose photophysics in solution and in the solid state has been more widely studied [2]. In addition to the monomer band, fluorescence emission of PVCz consists of two excimer species that appear at ~370 nm and ~420 nm. Such species arise from those conformations where face-to-face carbazole (Cz) groups partially and totally overlap [2–7]. Photophysical processes like energy transfer and/or energy migration and excimer formation significantly influence its photoconductive properties. Energy migration is an important way for increasing the excimer population sites, but at the same time these excimers act as traps for this energy migration decreasing the efficiency of energy transfer and therewith photoconduction [8–13]. Decreasing the excimer-forming sites without diminishing the chromophore density would be an ideal manner for improving the efficiency of the carrier generation and photoconduction.

We have reported several studies on energy transfer and energy migration for homopolymers (polyesters), some copolymers and bi- and trichromophoric model compounds with different chromophore types [13–22]. These studies are usually a combination of experiments and molecular modeling. Theoretical calculations allow us to rationalize the efficiency of experimentally obtained energy transfer between chromophores by assuming the experimental Förster radius. One of our most recent works [22] was performed on polyphosphazenes containing phenoxy and binaphthoxy chromophoric groups. Results suggested that 100% of the excitation energy of the phenoxy groups is transferred to the binaphthoxy groups

* Corresponding author. Tel.: +34 91 8854672; fax: +34 91 8854763.
E-mail address: francisco.mendicuti@uah.es (F. Mendicuti).

0032-3861/$ - see front matter © 2006 Elsevier Ltd. All rights reserved.
doi:10.1016/j.polymer.2006.08.039

and that this energy migrates among binaphthoxy groups along the polymer chain. The lack of binaphthoxy excimers, due to the non-stability of such excimers [23], makes the energy migration to increase monotonically with the content of binaphthoxy groups. However, the studies of the energy transfer between Cz groups in *N*-vinyl carbazole/MMA copolymers suggested that the chains with the highest Cz content do not show the highest efficiency for the singlet-energy transfer. Intramolecular excimers, which are mainly due to Cz–Cz sequences in the polymer chain, act as energy migration traps [13].

This work reports a study of the intramolecular singlet-energy transfer between Cz groups for *N*-vinyl carbazole/styrene copolymers of different monomer compositions. Fluorescence anisotropy and quenching by CCl_4 measurements for dilute solutions of the samples in a rigid PMMA matrix and in THF, respectively, allow us to obtain parameters related to the efficiency for the energy transfer process between Cz chromophores and their dependence on the number-average sequence length of the styrene units. Molecular dynamics simulations were also performed on isotactic and syndiotactic trichromophoric oligomers of the type CH_3–A–CH_2–B_m–A–CH_2–B_m–A–CH_3 where A = –CHCz–, B = –CH(C_6H_5)–CH_2– and $m = 0$–5, 10 and 15, with the objective of rationalizing the experimental behavior.

2. Materials, instrumentation and methods

2.1. Samples and solvents

Poly(*N*-vinyl carbazole), PVCz and *N*-vinyl carbazole/styrene copolymers were synthesized from *N*-vinyl carbazole (VCz, Aldrich, 98%, recrystallized ×2 from methanol) and styrene (ST, Merk 99%, distilled under vacuum) monomers by free radical polymerization in the presence of AIBN (Across, 98%) as described elsewhere [7]. In brief: a toluene deoxygenated (15 min bubbling with N_2) solution mixture of VCz, ST and AIBN (10^{-3} g/g of reactive mixture of monomers) was heated under N_2 atmosphere (70 °C, 10 h). The content was precipitated in cold methanol (Panreac, reagent grade) and filtered. The product was washed several times with petroleum ether (Scharlau, reagent grade). It was then precipitated (×2) from *p*-dioxane into petroleum ether in an ice bath. After 20 h it was again filtered and dried (vacuum, at ~30 °C). Purity was checked by UV/vis and ^{1}H NMR.

In the remainder of the manuscript copolymers will be sequentially identified from P1 to P11 where the digit increases as the carbazole (Cz) content decreases. P0 and P12 are assigned for PVCz and polystyrene (PS) homopolymers, respectively. Composition determined by elemental analysis of N, C and H content provides: P1 (N = 6.90, C = 86.96, H = 5.81); P2 (N = 6.29, C = 85.79, H = 6.17); P3 (N = 4.96, C = 87.75, H = 6.63); P4 (N = 4.63, C = 88.32, H = 6.53); P5 (N = 3.66, C = 88.58, H = 7.19); P6 (N = 3.40, C = 88.43, H = 7.23); P7 (N = 2.74, C = 89.41, H = 7.39); P8 (N = 1.77, C = 90.15, H = 7.25); P9 (N = 1.54, C = 90.45, H = 7.30); P10 (N = 0.78, C = 89.12, H = 7.39); P11 (N = 0.18, C = 91.97, H = 7.75). The monomer reactivity ratios (MRR) of VCz(r_1) and ST(r_2) were obtained by Fineman–Ross [24] and Kelen–Tüdos [25]. Both methods gave analogous values; $r_1 = 0.10$, $r_2 = 6.31$ and $r_1 = 0.16$, $r_2 = 7.18$, respectively, and they are also very similar to the ones reported previously by us [7]. The dependence of the copolymer composition on the monomers feed is depicted in Fig. 1. Table 1 collects the feed and copolymer compositions, and the number-average sequence length of the VCz($\overline{n}_1$) and the ST($\overline{n}_2$) monomer units [26].

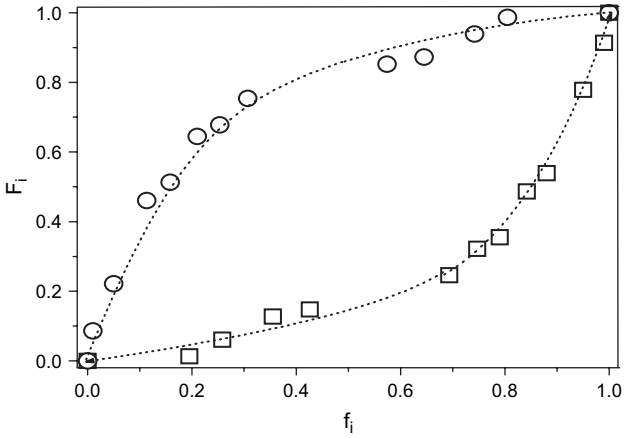

Fig. 1. Composition diagram for *N*-vinyl carbazole/styrene copolymerization: f_i mol fraction of i monomer in feed; F_i mol fraction of i monomer in copolymer [VCz(□) and ST(○)].

Ethylcarbazole (ECz, Aldrich, 98%, recrystallized ×2 from methanol) and ethylbenzene (EBz, Fluka, >99%, as received) were used as model compounds. Commercial PS (Aldrich, MW = 32,600) was used as P12. Methyl methacrylate (MMA stabilized with methylhydroquinone, Acros, 99%) distilled under vacuum was used for the preparation of the dilute polymer solutions in glassy PMMA matrices. CCl_4 used as fluorescence quencher (Aldrich, spectrophotometric grade), THF (Aldrich, spectrophotometric grade) and MMA (previously distilled under vacuum) were checked for impurities by fluorescence before using.

The preparation of the diluted polymer PMMA solid samples was carried out as follows [14]: ~3 mL of a fresh solution of the polymer (absorbance ~0.3 at 294 nm) in the distilled

Table 1
Feed (f) and copolymer (F) compositions, and number-average sequence length, $\overline{n}$ of VCz(1) and ST(2) in copolymers

Polymer	f_1	f_2	F_1	F_2	$\overline{n}_1$	$\overline{n}_2$
P0 (PVCz)	1.000	0.000	1.000	0.000	∞	0.0
P1	0.990	0.010	0.914	0.086	14.1	1.1
P2	0.950	0.050	0.779	0.221	3.5	1.4
P3	0.880	0.113	0.539	0.461	2.0	1.9
P4	0.842	0.158	0.487	0.513	1.7	2.3
P5	0.790	0.210	0.355	0.645	1.5	2.8
P6	0.747	0.253	0.322	0.678	1.4	3.3
P7	0.693	0.307	0.246	0.754	1.3	4.0
P8	0.426	0.574	0.148	0.852	1.1	10.1
P9	0.355	0.645	0.127	0.873	1.1	13.2
P10	0.258	0.742	0.061	0.939	1.0	20.4
P11	0.195	0.805	0.013	0.987	1.0	28.8
P12 (PS)	0.000	1.000	0.000	1.000	0.0	∞

MMA were introduced into a test tube ($\varnothing = 22.5$ mm). O_2 was removed by immersing the tubes in an ultrasonic bath (30 min) followed by dry N_2 bubbling through the solution (12 min). Polymerization was carried out in the presence of AIBN ($\sim 10^{-3}$ g/g MMA, at 65 °C for 19 h). Transparent solid samples were retrieved by breaking the test tube.

2.2. Instrumentation and methods

Absorption spectra were recorded in a Lambda 35, Perkin Elmer UV/vis spectrophotometer. Steady-state fluorescence measurements were performed with a SLM 8100 Aminco spectrofluorometer equipped with a Xe lamp, a double monochromator in the excitation and emission paths and a cooled Peltier system photomultiplier. Excitation and emission slit widths were 8 nm. Polarizers were set to magic-angle conditions. Fluorescence decay measurements were performed on a TCSPC FL900 Edinburgh Instruments spectrometer, equipped with a thyratron gated lamp filled with H_2, two concave gratings monochromators at both the excitation and emission paths, and a red-sensitive photomultiplier immersed in a Peltier cooled housing. Slits were set to 18 nm bandwidth. The data acquisition was carried out with 1024 channels and a time window width of 125 ns with a total of 10,000–15,000 counts in the peak. Instrumental response functions were regularly achieved by measuring the scattering of a Ludox solution. Intensity fluorescence profiles were fitted to the usual multi-exponential decay functions by the iterative reconvolution method [27] as

$$I(t) = \sum_i A_i e^{-t/\tau_i} \tag{1}$$

where A_i is the pre-exponential factor of the component with a lifetime τ_i of the multi-exponential function intensity decay.

Right-angle geometry, rectangular 10-nm path cells and a temperature of 25 °C were used for the measurements in aerated dilute fluid solutions. Absorbances at the excitation wavelength of 294 nm (only Cz groups excited) were in the 0.1–0.2 range. Solvent baselines were measured and subtracted from the steady-state fluorescence signal. Front-face illumination, an incident beam forming 60° with the surface and room temperature, was used for fluorescence depolarization measurements of the polymer PMMA solid samples. The estimated polymer concentration in fluid solution was very small, around $4–7 \times 10^{-3}$ g/L, to avoid intermolecular interactions. The concentration in the PMMA matrix was approximately one order of magnitude larger.

The fluorescence depolarization measurements for the samples in solution were obtained by the well-known "Single-Channel or L-format" method [28]. Thus the anisotropy r was defined as:

$$r = (I_{VV} - GI_{VH})/(I_{VV} + 2GI_{VH}) \tag{2}$$

where I_{xy} is the intensity of the emission that is measured when the excitation polarizer is in the position x (V for vertical, H for horizontal), the emission polarizer is in the position y, and the G factor ($=I_{HV}/I_{HH}$) corrects for any depolarization produced by the optical system. For dilute solutions of polymers in a rigid medium, where rotational diffusion and conformational change rates are diminished, a decreasing of the fluorescence anisotropy means an increasing of energy transfer.

Fluorescence quenching has also been used to estimate the efficiency in the intramolecular transfer and energy migration processes in polymers, including those containing Cz groups, dispersed in dilute fluid solutions [12,13,29–31]. If an individual excited species is quenched by dynamic quenching with a quencher Q, the steady-state Stern–Volmer quenching constant K_{SV}, which provides a measure of the efficiency of quenching, is given by

$$\frac{F}{F_0} = 1 + K_{SV}[Q] = 1 + k_Q \tau_0 [Q] \tag{3}$$

where F_0 and F are the values of fluorescence quantum yield (ϕ), intensity (I) or lifetime (τ) in the absence and presence of a given concentration of quencher $[Q]$, k_Q is the bimolecular quenching constant, and τ_0 is the excited-state lifetime in the absence of Q. Eq. (3) is strictly applicable to the quenching of an individual species [32].

For P# excited states whose fluorescence intensity decays are multi-exponential, τ is usually taken as a weighed average of the individual components of decay function as

$$\langle \tau \rangle = \frac{\sum_i A_i \tau_i^2}{\sum_i A_i \tau_i} \tag{4}$$

Eq. (4) assumes that each lifetime component is due to independent species. Assuming that each component is independently quenched with the same k_Q, then F_0/F is related to the $[Q]$ as [13]:

$$\frac{F}{F_0} = 1 + k_Q \langle \tau \rangle_0 [Q] \tag{5}$$

The modified Smoluchoswki–Einstein [33] equation can be used to interpret k_Q:

$$k_Q = 4 N_A R \left(D_C + D_Q + \Lambda_m \right) \gamma \tag{6}$$

where D_C and D_Q are the diffusion coefficients of the excited chromophore and quencher, respectively ($D_{CCl_4} \approx 1.51 \times 10^{-5}$ cm^2 s^{-1}) [34]; R is the collisional radius for the excited species and Q, Λ_m is the singlet-energy migration coefficient and γ is the quenching probability per collision. Assuming that γ and R are the same in all polymer samples, $D_C \approx 0$ for Cz linked to the polymers and that $\Lambda_m \approx 0$ for the copolymer with the smaller Cz content, P11.Then the following equation is obtained

$$\Lambda_m = D_{CCl_4} \left(\frac{k_Q^{P\#} - k_Q^{P11}}{k_Q^{P11}} \right) \tag{7}$$

Λ_m is directly related to the Cz–Cz efficiency of energy transfer.

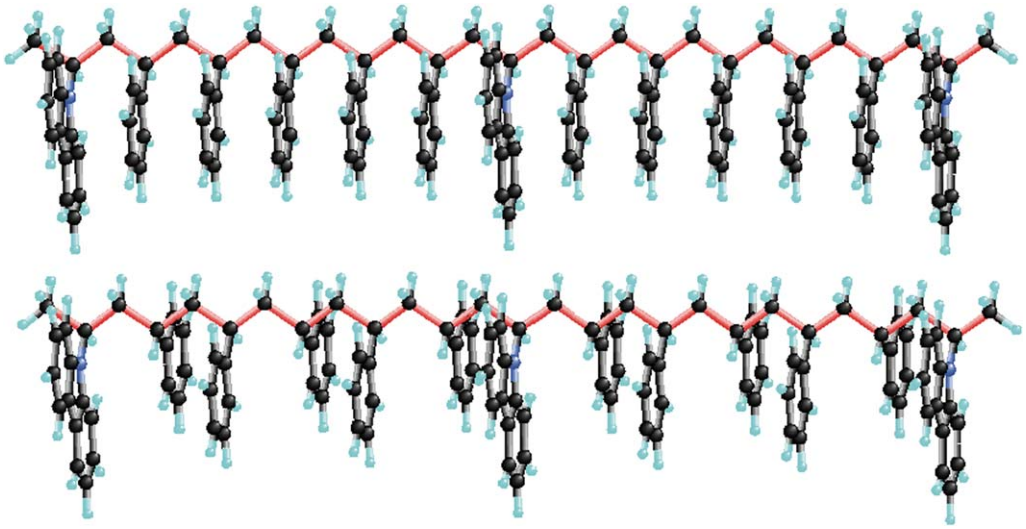

Fig. 2. Initial *trans* conformation for the isotactic and syndiotactic fragments ($m = 5$) simulated by MD.

2.3. Molecular dynamics (MD) details

The 1 ns MD simulations were performed at 600 K by using Sybyl 6.6 [35] with ground state parameters of Tripos Force Field [36]. As MRR are $r_2 \gg r_1$, the calculations were carried out on (100%) isotactic and syndiotactic oligomers containing three VCz units separated by 1–5, 10 and 15 ST ones. Fragments, one of them being depicted in Fig. 2, are of the type $CH_3{-}A{-}CH_2{-}B_m{-}A{-}CH_2{-}B_m{-}A{-}CH_3$ where $A = -CHCz-$, $B = -CH(C_6H_5){-}CH_2-$ and $m = 0$–5, 10 and 15. For the potential energy the sum of bond stretching, angle bending, torsional, van der Waals, electrostatics and out-of-plane energy contributions were assumed. The simulations were started on minimized (simplex algorithm, conjugate gradient with 0.2 kcal/mol Å) all *trans* conformations similar to the one depicted in Fig. 2. The probability of the conformations which satisfy some special requirements is obtained as the fraction of these conformations from total ones. More details about, charges, geometry and methods were reported elsewhere [7].

Three parameters related to the Cz–Cz energy transfer efficiency from the analysis of the trajectories of trichromophoric fragments were calculated, namely:

(a) The probability $P(R)$ of finding the center of the pyrrole ring of one Cz′, involved in the Cz–Cz′ interaction, within a sphere of radius R centered at the center of pyrrole ring of Cz group.
(b) The $\kappa^2 P(R)$ product, where κ^2 is the orientational factor for fixed absorption and emission dipole transition moments along the axis passing through the center of the pyrrole ring and N atom. Both $P(R)$ and $\kappa^2 P(R)$ parameters were the normalized sum of two possible Cz–Cz adjacent interactions.
(c) The efficiency of the energy transfer process can be obtained as

$$\Phi_{ET} = \frac{1}{2N}\sum_{i=1}^{N}\left(1 + \frac{(2/3)R^6}{\kappa^2 R_0^6}\right)^{-1} \quad (8)$$

R_0 is the experimental Cz–Cz Förster radius value of 20 Å obtained previously [13].

3. Results and discussion

3.1. Fluorescence measurements

Fig. 3 depicts absorption spectra for ECz and EBz model compounds and one copolymer (P4). Other P# shows features similar to those of P4, with distinguishable bands around 262, 294, 331 and 345 nm in THF. Homopolymers P0 and P12 show spectra very similar to ECz and EBz model compounds, respectively. The location of the bands does not seem to significantly change upon changing copolymer composition.

Fig. 4 shows emission spectra for ECz and P0–P11 in THF fresh dilute solutions and in the solid PMMA matrix upon excitation at 294 nm, wavelength at which only the Cz groups are excited. The spectra for ECz exhibit peaks located at

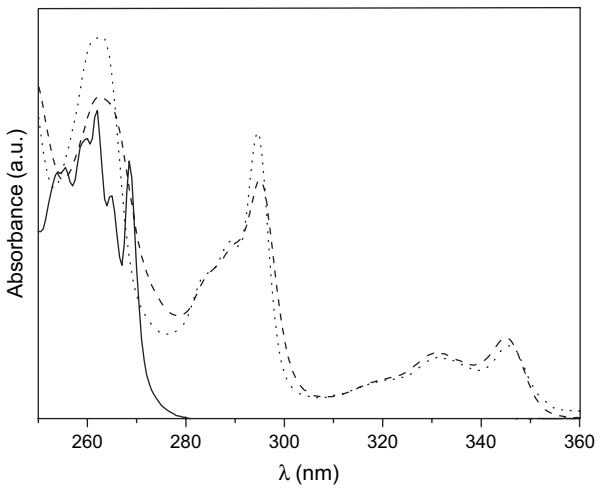

Fig. 3. Absorption spectra for EBz (—), ECz (- - -) and copolymer P4 (— —) in THF at 0 °C.

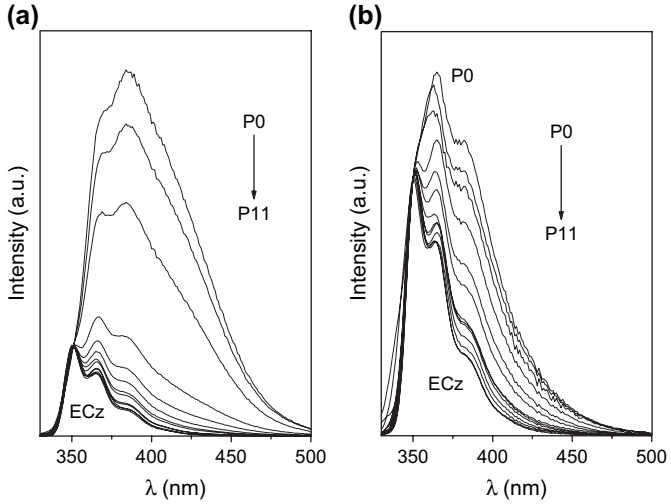

Fig. 4. Emission spectra for P# and ECz normalized at the maximum of monomer band observed for ECz. Spectra are collected for (a) dilute solutions in THF and (b) ECz and P#-PMMA solid samples at room temperature. Excitation is at 294 nm.

∼352 and ∼367 nm, with a shoulder at ∼385 nm. The spectra for P0–P11 are normalized at the maximum of the monomer high energy band obtained for ECz. Emission spectra for P0–P11 show a broadening to the red of the monomer band observed for ECz. This broadening, which is more evident for the first members of the P# series ($\bar{n}_1 > 2$), is due to intramolecular excimer emission. The placement and relative intensities of the excimer bands depend on the composition of the copolymer and on the nature of the medium. In general the excimer emission intensity monotonically decreases as the Cz content decreases. The last four members of the copolymer series, P8–P11, have emission characteristics very similar to those seen with ECz. These four copolymers have a VCz unit content below 15 mol% and their number average sequences of VCz and ST units are $\bar{n}_1 \approx 1$ and ($\bar{n}_2 > 10$), respectively (Table 1). The VCz units tend to be quite separate in P8–P11. These results indicate, as with other carbazole copolymers [6,7,13], that Cz–Cz sequences are responsible for most of the excimers. Another observation is that chain dynamics significantly contributes to the intramolecular excimer population as the amount of excimers for P# is always considerably larger in the fluid media than in the rigid PMMA.

EBz emission spectrum show a single band located at ∼285 nm, PS, however, exhibits bands placed at ∼285 and 335 nm from the monomer and excimer emissions, respectively. When P1–P11 are excited at 262 nm (both Bz and Cz chromophores are simultaneously excited) normalized emission spectra are very similar to the one obtained upon 294 nm excitation. No emission at all is obtained from ST units. This takes place whatever the composition and the solvent used. Results indicate a 100% efficiency for Bz → Cz energy transfer.

The left panel of Fig. 5 depicts the excitation spectrum for ECz and the excitation anisotropy spectra for ECz, P0 as well as some copolymers measured in the solid PMMA matrix at room temperature with emission fixed at 367 nm. This wavelength was placed at one peak, 17 nm toward the red of the monomer band to avoid interference from scattered exciting light. Excitation spectra for P# are very similar and exhibit characteristics matching the absorption spectra, showing bands placed (in the wavelength range shown) at approximately 294, 332 and 344 nm. Bands placed at ∼345 and 295 nm for Cz are the (0,0) transitions from the ground to the first and second excited singlet states of Cz. They are known as $^1L_b \leftarrow {}^1A$ and $^1L_a \leftarrow {}^1A$ transitions, respectively [37,38]. For these electronic transitions, the absorption oscillators are in the plane of

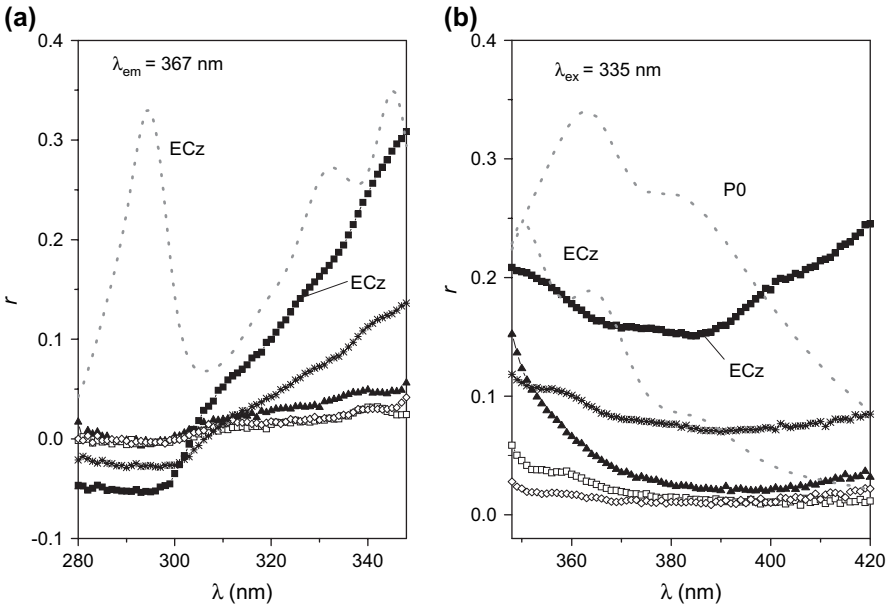

Fig. 5. (a) Fluorescence excitation anisotropy spectra for ECz, P0 homopolymer and P4, P7 and P11 copolymers in the PMMA solid matrix obtained with the emission at 367 nm. The dashed line depicts the excitation spectrum for the ECz sample at the same experimental conditions and (b) fluorescence emission anisotropy spectra upon excitation at 335 nm for ECz, P0, P4, P7 and P11 and emission spectra (dashed lines) for ECz and P0 in the PMMA solid matrix at room temperature. Symbols correspond to: ECz (■), P0 (▲), P4 (□), P7 (◇), P11 (∗).

Table 2
Average of the anisotropies $\bar{r}$ at different pairs of excitation and emission wavelengths where $^1L_b \leftarrow {}^1A$ and $^1L_b \rightarrow {}^1A$ transitions are involved, obtained from the emission and excitation spectra of the vitrified ECz, P0–P11 PMMA samples

	$\lambda_{em} = 352$, $\lambda_{ex} = 333 \pm 5$	$\lambda_{em} = 367$, $\lambda_{ex} = 345 \pm 5$	$\lambda_{em} = 367$, $\lambda_{ex} = 332 \pm 5$	$\lambda_{ex} = 335$, $\lambda_{em} = 350 \pm 5$	$\lambda_{ex} = 335$, $\lambda_{em} = 364 \pm 5$
ECz	0.192 ± 0.034	0.287 ± 0.025	0.177 ± 0.022	0.209 ± 0.017	0.168 ± 0.008
P0	0.099 ± 0.022	0.052 ± 0.009	0.038 ± 0.005	0.166 ± 0.115	0.053 ± 0.010
P1	0.154 ± 0.054	0.041 ± 0.003	0.040 ± 0.001	0.200 ± 0.170	0.039 ± 0.009
P2	0.090 ± 0.018	0.033 ± 0.010	0.037 ± 0.004	0.152 ± 0.096	0.051 ± 0.011
P3	0.016 ± 0.005	0.014 ± 0.006	0.008 ± 0.002	0.042 ± 0.059	0.009 ± 0.002
P4	0.037 ± 0.009	0.028 ± 0.003	0.020 ± 0.003	0.067 ± 0.052	0.028 ± 0.006
P5	0.026 ± 0.006	0.022 ± 0.003	0.016 ± 0.002	0.051 ± 0.044	0.021 ± 0.004
P6	0.031 ± 0.007	0.027 ± 0.002	0.019 ± 0.002	0.064 ± 0.048	0.032 ± 0.005
P7	0.039 ± 0.012	0.036 ± 0.010	0.022 ± 0.002	0.036 ± 0.037	0.014 ± 0.002
P8	0.027 ± 0.009	0.018 ± 0.005	0.011 ± 0.002	0.035 ± 0.037	0.015 ± 0.001
P9	0.026 ± 0.006	0.029 ± 0.006	0.017 ± 0.002	0.040 ± 0.036	0.019 ± 0.002
P10	0.043 ± 0.006	0.054 ± 0.007	0.040 ± 0.003	0.059 ± 0.034	0.044 ± 0.002
P11	0.110 ± 0.020	0.128 ± 0.010	0.079 ± 0.010	0.122 ± 0.027	0.092 ± 0.007

Values of $\bar{r}$ are obtained from the averages of r in the range of 10 nm around the specified values of the excitation and emission wavelengths (in nm).

the ring system and perpendicular to each other. The fact that the Cz monomer emission (0,0) band corresponds to a $^1L_b \rightarrow {}^1A$ transition is a consequence of the anisotropy signs at the excitation wavelength of ~295 nm ($r < 0$) or ~345 nm ($r > 0$) when the emission is fixed to the maximum of the monomer band or close to it, as shown in the left panel of Fig. 5. However, whatever the anisotropy signs, P0–P11 exhibit absolute values of r at the wavelength of such transitions that are smaller than those for the ECz model compound. The value of r strongly depends on the copolymer composition. The right panel of Fig. 5 depicts the emission spectra for ECz and P0 and the emission anisotropy spectra for ECz, P0 as well as some copolymers upon excitation at 335 nm. The "intrinsic" parallel orientation of the absorption and emission transition moments is also responsible for the positive r values observed for the anisotropy emission spectra. The largest r value is again obtained for ECz. P0–P11 always have smaller values.

Table 2 lists the values of $\bar{r}$ for ECz and P#-PMMA solid samples at different pairs of excitation–emission wavelengths where $^1L_b \leftarrow {}^1A$ and $^1L_b \rightarrow {}^1A$ transitions are involved. Such data were obtained by sampling over a 10-nm window centered on the wavelength stated. The largest anisotropy values were obtained for the ECz model, for which energy transfer at this chromophore concentration is not possible. In a rigid medium the degree of depolarization is related to the extent of energy transfer or migration between chromophores attached to a polymer chain, the isotropy, r^{-1}, being proportional to the extent of this process.

The three panels in Fig. 6 show the isotropy values for P0–P11 relative to that for the ECz, $\bar{r}_{P\#}^{-1}/\bar{r}_{ECz}^{-1}$ as a function of $\bar{n}_2$ obtained at different excitation–emission wavelength pairs. Absolute values of $\bar{r}_{P\#}^{-1}/\bar{r}_{ECz}^{-1}$ obviously depend on the selected wavelengths, but plots look very similar. P0 and the first members of the series with the largest Cz content and Cz–Cz sequences do not show the highest $\bar{r}_{P\#}^{-1}/\bar{r}_{ECz}^{-1}$. In fact, $\bar{r}_{P\#}^{-1}/\bar{r}_{ECz}^{-1}$ initially seems to increase monotonically with $\bar{n}_2$ from P0($\bar{n}_2 = 0$) until somewhere between P4 and P7($\bar{n}_2 \approx 2$–4 and $\bar{n}_1 \leq 2$) and it definitely decreases from P8($\bar{n}_2 \approx 10$) through P11($\bar{n}_2 \approx 29$). The largest $\bar{r}_{P\#}^{-1}/\bar{r}_{ECz}^{-1}$ ratios, and therefore the highest efficiency for Cz–Cz energy transfer, are obtained for the polymers that have the highest Cz content but hardly have Cz–Cz sequences. Cz–Cz

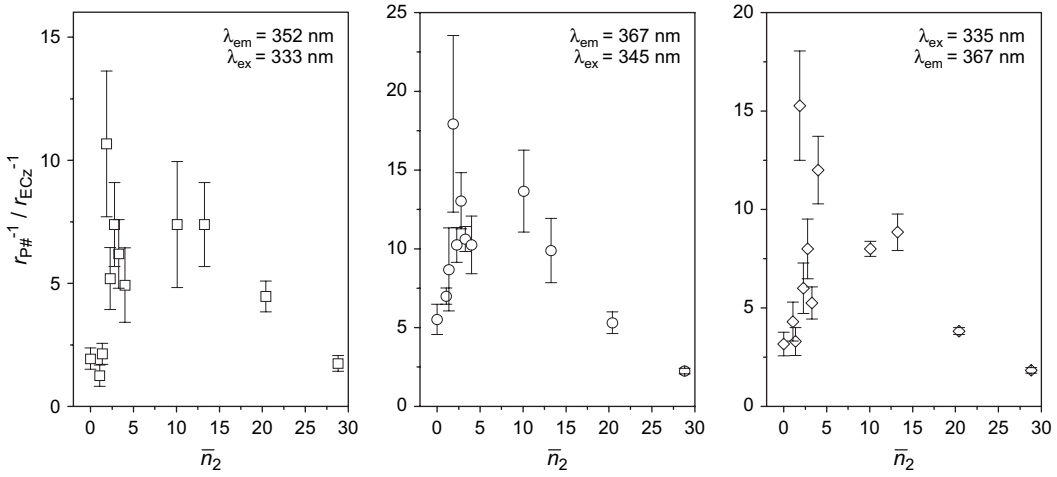

Fig. 6. Average of the isotropy values relative to the one for the ECz model compound, $\bar{r}_{P\#}^{-1}/\bar{r}_{ECz}^{-1}$ vs. $\bar{n}_2$ for P0–P11 in vitrified PMMA at the specified excitation and emission wavelengths. $\lambda_{ex} = 333$ nm, $\lambda_{em} = 352$ nm (□); $\lambda_{ex} = 345$ nm, $\lambda_{em} = 367$ nm (○); $\lambda_{ex} = 335$ nm, $\lambda_{em} = 367$ nm (◇). Averages were obtained from Table 2.

sequences are mostly responsible for the excimer formation [6,7].

Fluorescence anisotropy r was also obtained upon simultaneous excitation of the Bz and Cz chromophores (262 nm) by fixing the ECz monomer band emission (354 nm). The value for ECz is negative ($r = -0.1385 \pm 0.0005$). The ones for P0–P11 seem to slightly decrease upon increasing the ST content ($r_{P_0} = -0.0317 \pm 0.0023$ and $r_{P_{11}} = -0.0449 \pm 0.0003$). The interpretation of this behavior is not easy, as several energy transfer processes (Bz → Bz, Bz → Cz and Cz → Cz), which depend on polymer composition, are involved.

Quenching experiments for ECz and P0–P11 in THF at 25 °C by CCl_4 were carried out by selecting 352 and 386 nm as emission wavelengths upon excitation at 262 and 294 nm. Analysis was achieved from lifetime measurements. Stern–Volmer plots, $\langle\tau\rangle/\langle\tau_0\rangle$ vs. [CCl_4] for ECz and P#, which are not shown, were reasonably linear in the whole [CCl_4] (0–60 mM) range. Table 3 lists the values of K_{SV} constants as well as lifetime averages in the absence of the quencher, $\langle\tau_0\rangle$ obtained with Eq. (4), at the two emission wavelengths where the monomer and the excimer are dominant. Fluorescence decays for ECz in the absence (or presence) of quencher upon excitation at 294 nm, when the emission is monitored at 352 or 386 nm are mono-exponential, with very similar lifetimes (~9 ns at [CCl_4] = 0). P0 and copolymers show more complicated decays which can be fit to three-exponentials. P0 (at [CCl_4] = 0), shows three lifetimes of 0.9 ns (1.3 ns), 5.1 ns (6.2 ns) and 19.0 ns (19.0 ns) at the emission of 352 nm (386 nm). For P1–P11, when decreasing (increasing) the VCz (ST) content several facts are observed: (a) the fastest component increases from 0.9 ns (P0) up to the value of 6–8 ns (P11), but its contribution decreases from 60–65% (P0) up to 10–20% (P11); (b) the intermediate component increases from the value of 5–6 ns (P0) up to the value of ~13 ns for P11. Its contribution also increases from ~20% up to 70–80% (P11); and (c) the slowest component, which does not have any special trend, maintains its value in a wide 19–28 ns range and its contribution decreases from 15–20% up to 0 for the last member of the series. This last component, because its contribution increases upon increasing emission wavelength and hardly appears for the member of the series with less Cz content, can be attributed to the excimers. The fastest one could be ascribed to the monomers that are part of Cz–Cz sequences and which are quenched by excimer formation. Their contribution is obviously more important for the first members of P# series. Several authors attribute the intermediate one to the isolated Cz units along the chain. The decreasing of the component for the copolymers with higher Cz content is due to the enhancing in quenching by the Cz–Cz energy transfer. This explanation is quite similar to the one proposed by other authors including us [5,13] for other Cz containing copolymer systems.

Table 3
Stern–Volmer constants, K_{SV} and average lifetime in the absence of quencher, $\langle\tau_0\rangle$ upon excitation at 262 and 294 nm by collecting the emission at 352 and 386 nm (italic)

Sample	K_{SV} (M^{-1})		$\langle\tau_0\rangle$ (ns)	
	$\lambda_{ex} = 262$ nm	$\lambda_{ex} = 294$ nm	$\lambda_{ex} = 262$ nm	$\lambda_{ex} = 294$ nm
ECz	82.6 ± 1.3	67.7 ± 5.6	10.9	8.2
	70.3 ± 0.1	*76.7 ± 5.8*	*9.8*	*9.0*
P0	68.7 ± 0.9	101.7 ± 6.1	9.6	12.8
	65.6 ± 1.0	*92.8 ± 3.9*	*11.1*	*14.1*
P1	74.4 ± 1.2	75.0 ± 1.0	9.3	9.2
	74.4 ± 1.3	*78.5 ± 1.3*	*11.2*	*11.8*
P2	100.1 ± 2.2	122.3 ± 3.9	10.3	12.3
	108.6 ± 3.3	*129.7 ± 4.8*	*14.0*	*16.3*
P3	70.9 ± 1.8	80.9 ± 2.1	7.1	8.0
	74.5 ± 1.1	*80.8 ± 2.0*	*9.9*	*10.7*
P4	148.1 ± 9.8	82.0 ± 2.5	14.7	9.1
	79.8 ± 2.6	*94.7 ± 4.1*	*11.0*	*12.7*
P5	52.3 ± 1.4	57.0 ± 2.5	6.6	7.1
	62.7 ± 2.6	*65.5 ± 3.9*	*8.8*	*9.2*
P6	96.6 ± 6.1	96.2 ± 6.2	11.7	11.8
	104.3 ± 8.2	*106.5 ± 8.1*	*14.4*	*14.6*
P7	61.2 ± 3.0	92.2 ± 8.1	8.2	10.6
	72.8 ± 3.1	*95.4 ± 6.3*	*10.2*	*12.9*
P8	68.1 ± 4.0	68.9 ± 3.1	11.0	10.8
	73.0 ± 4.0	*72.4 ± 3.5*	*11.9*	*11.8*
P9	81.4 ± 4.8	80.9 ± 4.8	12.6	12.5
	85.6 ± 5.7	*85.7 ± 5.7*	*13.8*	*13.7*
P10	75.9 ± 7.1	74.9 ± 6.5	13.7	13.4
	77.8 ± 7.7	*76.9 ± 7.1*	*14.4*	*14.0*
P11	56.4 ± 3.1	66.1 ± 1.2	12.8	13.0
	25.5 ± 1.5	*56.8 ± 1.8*	*7.10*	*11.8*

Fig. 7 depicts singlet-energy migration rate Λ_m (cm s^{-1}) values obtained by using Eq. (7) for several pairs of excitation and emission wavelengths vs. the number-average sequence length $\bar{n}_2$. All polymer samples (with the exception of P11 which was taken as a model with $\Lambda_m = 0$) show values of $\Lambda_m > 0$. These results also indicate the presence of energy transfer processes along the polymer chain which strongly depend on $\bar{n}_2$. Λ_m seems to show a similar trend with $\bar{n}_2$ as the fluorescence isotropy. Λ_m and, therefore, the efficiency of energy transfer increases with $\bar{n}_2$ for the first members and decreases for the ones with smallest Cz content. The maximum Λ_m takes place for the intermediate members of the P# series. P0 and copolymers with the highest number of Cz–Cz sequences, with the highest excimer formation, do not show the highest energy transfer rate.

3.2. Molecular dynamics

Left panel of Fig. 8 shows the dependence of $P(R)$, $\kappa^2 P(R)$ and the efficiency Φ_{ET} on m for $R_0 = 20$ Å, the value of Förster radius for Cz–Cz transfer [13]. When $R = R_0$, $P(R)$ and $\kappa^2 P(R)$ take the value of 1 for $m = 1$–5 for both the isotactic and syndiotactic fragments. Both parameters are considerably smaller for $m = 10$ and 15. Thus energy transfer should be possible for all conformations of $m = 1$–5 fragments. Obviously this does not happen for $m = 10$ and 15.

Fig. 8 (left) also shows the efficiency of the Förster transfer Φ_{ET} obtained from Eq. (8) as a function of m. Φ_{ET} decreases with m for both the isotactic and syndiotactic fragments. This decreasing, however, is slightly larger for the isotactic samples. This figure also depicts the probability of the conformations that can adopt a sandwich geometry (or excimer) between Cz groups [7]. Later results show that the probability

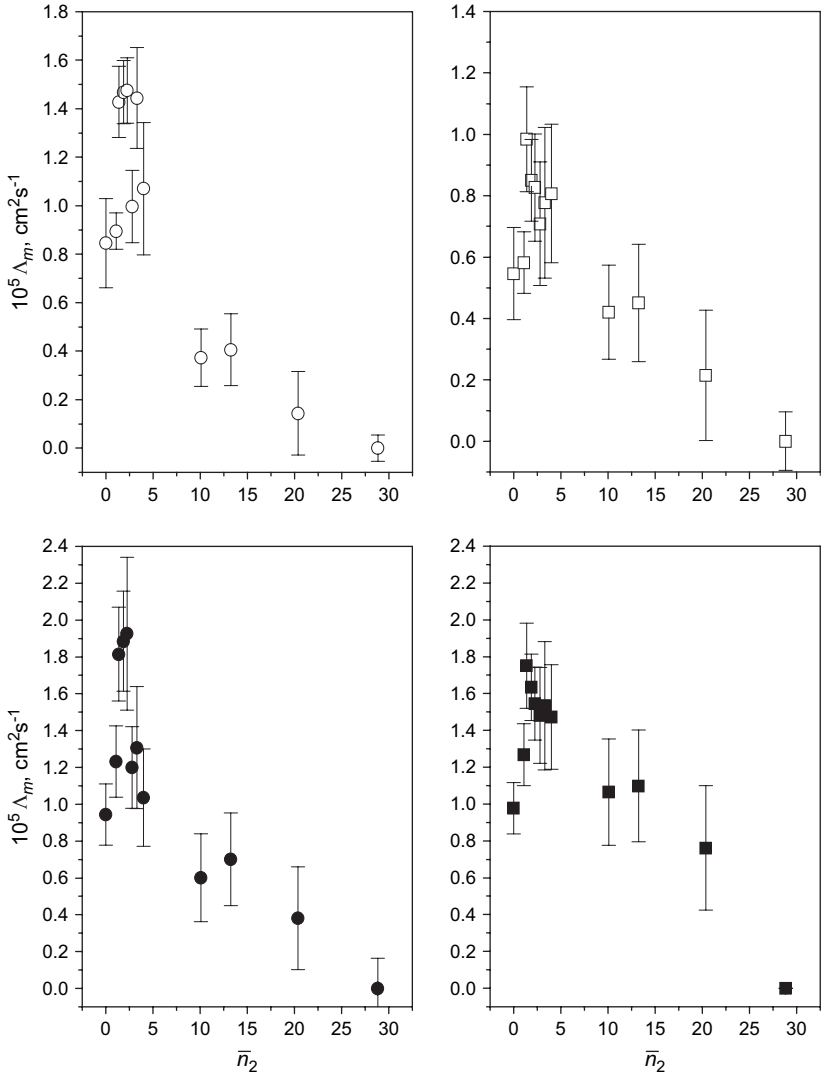

Fig. 7. Singlet-energy migration rate Λ_m (cm s^{-1}) vs. the number-average sequence length of ST monomer units $\bar{n}_2$, upon excitation at 294 nm by selecting the emission at 352 nm (○) or 386 nm (□) (upper panels) or upon excitation at 262 nm by monitoring the emission at 352 nm (●) or 386 nm (■) (bottom panels).

for excimer formation decreases monotonically with m and it is almost zero for $m > 2$. The highest probability for $m = 0$ agrees with the fact that the largest amount for intramolecular excimer formation occurs for P0. But the results also state that most of the excimers should be due to interaction between Cz groups in Cz–Cz adjacent sequences [7]. The probabilities for excimers are almost zero when more than two ST units are placed between Cz groups ($m > 2$).

Φ_{ET} calculations by Eq. (8) only take into account distances and orientations between carbazole groups and they do not consider the possibility that excimers could act as energy transfer traps. If this were true, the efficiency of energy transfer should be inversely proportional to the probability for excimer formation. The right panel of Fig. 8 shows the efficiency for the energy transfer process obtained in a similar manner by assuming that those conformations that fulfill the excimer requirements are not capable of transferring the energy. According to these results energy transfer may increase with m for $m \leq 2$ and therefore decrease for $m > 2$. This behavior is very similar to the experimental one. Experimentally the amount of intramolecular excimers decreases with $\bar{n}_2$ and the efficiency of energy transfer passes through a maximum somewhere around $\bar{n}_2 = 2$–4. For the polymers with a high content of Cz–Cz sequences, excimers act as energy traps, inhibiting the process of Cz–Cz energy transfer.

4. Conclusions

The analysis of emission spectra, fluorescence depolarization and quenching measurements on *N*-vinyl carbazole/styrene copolymers of different monomer compositions suggests that, upon excitation of carbazole groups (or benzene and carbazole simultaneously), an energy transfer process between carbazole groups along the polymer chain takes place. The efficiency of this process depends on copolymer composition. However, the highest efficiency does not seem to correspond to the copolymers with the highest carbazole content, i.e. with the highest excimer formation. Intramolecular excimers, which are mostly formed by interaction between adjacent carbazole chromophores, undoubtedly act as energy

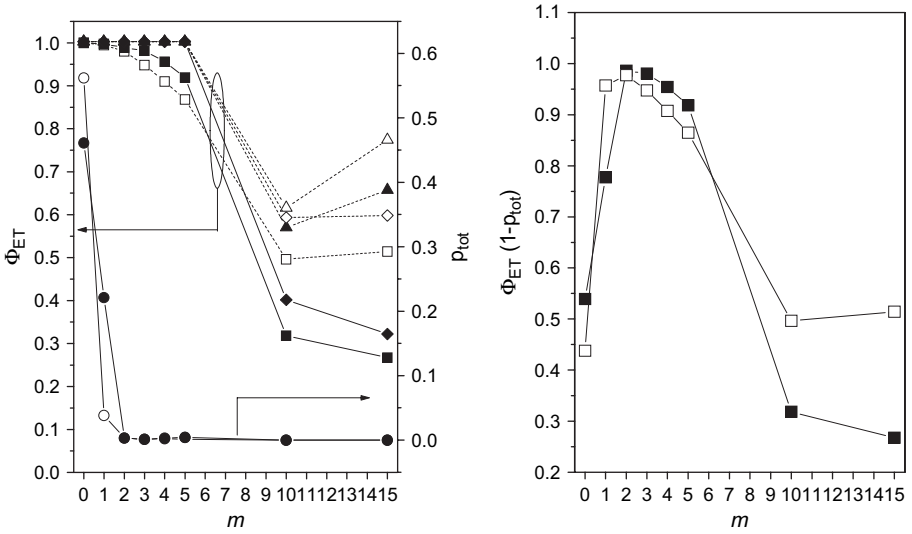

Fig. 8. Left: $P(R)$ (diamonds), $\kappa^2 P(R)$ (triangles) and the efficiency Φ_{ET} (squares) for the Cz–Cz Förster transfer for the experimental value of R_0 (20 Å) in isotactic (open symbols) and syndiotactic (filled symbols) fragments as a function of m. Values of probability (circles) of intramolecular excimers, p_{tot}, obtained from the analysis of MD simulations (Ref. [7]). Right: efficiency of energy transfer obtained under the assumption that the excimer-forming conformations are not capable of transferring the energy vs. m.

migration traps between carbazole groups. Molecular dynamics simulations analysis on isotactic and syndiotactic copolymer fragments supports most of the experiments. The results lead to the conclusion that an increase in the density of carbazole chromophores in the polymers chain does not always contribute in improving the efficiency of energy migration between them.

Acknowledgements

This research was supported by the Comunidad de Madrid (project S-055/MAT/0227), CICYT (project CTQ2005-04710/BQU). N. Gatica acknowledges the Centro de Investigación de Polímeros Avanzados (CIPA-Chile) for postdoctoral fellowship. We wish to express our thanks to M.L. Heijnen for assistance with the preparation of the manuscript.

References

[1] Law KY. Chem Rev 1993;93(1):449–86.
[2] Solaro R, Galli G, Ledwit A, Chiellini E. Fluorescence emission properties of optically active vinyl polymers containing carbazole and related aromatic units. In: Phillips D, editor. Polymer photophysics: luminescence, energy migration and molecular motion in synthetic polymers. New York: Chapman & Hall; 1985. p. 377–430.
[3] Johnson GE. J Chem Phys 1975;62:4697–709.
[4] Itaya K, Okamoto K, Kusabayashi S. Bull Chem Soc Jpn 1976;49:2082–8.
[5] Davidson K, Soutar I, Swanson L, Yin J. J Polym Sci Part B Polym Phys 1997;39:963–78.
[6] Gallego J, Pérez-Foullerat D, Mendicuti F, Mattice WL. J Polym Sci Part B Polym Phys 2001;39:1272–81.
[7] Sanz A, Mendicuti F. Polymer 2002;43:6123–30.
[8] Bai F, Chang CH, Webber SE. Macromolecules 1986;19:588–95.
[9] Bai F, Chang CH, Webber SE. Macromolecules 1986;19:2484–94.
[10] Morishima Y, Kobayashi T, Nozakura S, Webber SE. Macromolecules 1987;20:807–13.
[11] Yoshihiro I, Webber SE. Macromolecules 1989;22:2766–75.
[12] Grazulevicius JV, Soutar I, Swanson L. Macromolecules 1998;31:4820–7.
[13] Gallego J, Mendicuti F, Mattice W. J Polym Sci Part B Polym Phys 2003;41:1615–26.
[14] Mendicuti F, Saiz E, Mattice WL. Polymer 1992;33:4908–12.
[15] Gallego J, Mendicuti F, Saiz E, Mattice WL. Polymer 1993;34:2475–80.
[16] Sánchez-Camacho A, Pozuelo J, Mendicuti F, Mattice WL. J Fluoresc 1997;7:113–20.
[17] Martin O, Mendicuti F, Saiz E, Mattice WL. Comput Theor Polym Sci 1998;7:149–57.
[18] Bravo J, Mendicuti F, Saiz E, Mattice WL. J Fluoresc 1996;6:41–50.
[19] Bravo J, Mendicuti F, Saiz E, Mattice WL. Macromol Chem Phys 1994;195:3411–24.
[20] Mendicuti F, Saiz E, Bravo J, Mattice WL. Polym Int 1995;36:137–46.
[21] Bravo J, Mendicuti F, Saiz E, Mattice WL. Macromol Chem Phys 1996;197:1349–60.
[22] Marcelo G, Saiz E, Mendicuti F, Carriedo GA, García Alonso FJ, García Álvarez JL. Macromolecules 2006;39(2):877–85.
[23] Carriedo GA, Álvarez JLG, García Alonso FJ, Soto AP, Tarazona MP, Mendicuti F, et al. Macromolecules 2004;37(14):5437–43.
[24] Fineman M, Ross SD. J Polym Sci 1950;5:259–62.
[25] Kelen T, Tüdos F. J Macromol Sci Chem 1975;A9(1):1–27.
[26] Odian G. Principles of polymerization. 4th ed. New York: J. Wiley & Sons; 1981 [chapter 6].
[27] O'Connor DV, Ware WR, André JC. J Phys Chem 1979;83:1333–43.
[28] Lakowicz JR. Principles of fluorescence spectroscopy. 2nd ed. New York: Kluwer Academic/Plenum; 1999 [chapter 10].
[29] Arora KS, Overberger CG, Johnson CE. J Polym Sci Polym Phys Ed 1986;24:2275–92.
[30] Webber SE, Avots-Avotins PE, Deumié M. Macromolecules 1981;14:105–10.
[31] Cabaness WR, Lin LC. J Polym Sci Polym Chem Ed 1984;22:857–62.
[32] Lakowicz JR. Principles of fluorescence spectroscopy. 2nd ed. New York: Kluwer Academic/Plenum; 1999 [chapter 8].
[33] Voltz R, Laustrait G, Coche A. J Chim Phys Phys Chim Biol 1966;63:1253–60.
[34] Heisel F, Laustrait H. J Chim Phys Phys Chim Biol 1965;66:895–902.
[35] Sybyl 6.6. Tripos Associates, St. Louis: MO; 1999.
[36] Clark M, Cramer III RC, van Opdenbosch NJ. Comput Chem 1989;10:982–1012.
[37] Johnson GE. J Chem Phys 1974;78:1512–21.
[38] Platt JR. J Chem Phys 1949;17:484–95.